ACCSCIENCE PUBLISHING

Asian Journal of Water, Environment and Pollution

ORIGINAL RESEARCH ARTICLE

Removal of antimonite by low-temperature Fe-modified biochar

Jiumei Long and Dongsheng Zhou*

College of Resources and Environment, Zunyi Normal University, Zunyi, Guizhou, China

Abstract

High-temperature biochar (BC) has been extensively studied for treating wastewater contaminated with antimonite (Sb(III)). In contrast, low-temperature BCs are more energy-efficient and eco-friendly, making them more promising for remediating contaminated environmental media; however, their performance and mechanisms for Sb(III) removal remain largely unexplored. To provide a theoretical basis for remediating antimony–contaminated natural environments, the present study investigated the Sb(III) removal performance and underlying mechanisms of two low-temperature (300 °C) BCs, namely ferric chloride ($FeCl_3$) co-pyrolyzed BC (FB) and $FeCl_3$-impregnated pristine BC (FBC), with pristine BC (PBC) as the control. The Sb(III) removal performance was evaluated using adsorption kinetic and isotherm models, and the mechanisms were elucidated via adsorption experiments across a pH range of 3–10. Results showed that the maximum adsorption capacities of PBC, FB, and FBC were 12.93, 9.01, and 14.57 $mg \cdot g^{-1}$, with FBC exhibiting superior Sb(III) removal performance. The kinetic model indicated that Sb(III) removal by FB and FBC was dominated by chemisorption. Characterization of the solid phases in the adsorption systems showed that functional groups were mainly responsible for Sb(III) adsorption/oxidation at pH 3, whereas co-oxidation of ferrous iron (Fe(II)) and Sb(III) was dominant at pH 10. Moreover, at an initial Sb(III) concentration of 5 $mg \cdot L^{-1}$, the residual aqueous Sb(III) in FBC-treated adsorption systems ranged from 0.015 to 0.036 $mg \cdot L^{-1}$ over the pH range of 3–10, indicating FBC's high versatility in Sb(III) removal owing to its abundant functional groups and high Fe(II) content. Thus, FBC exhibits substantial potential to remediate Sb(III) contamination in environmental media across a typical environmental pH range of 3.0–10.0.

Keywords: Sb(III) remediation; Oxygen-containing functional group; Antimonite oxidation; Ferrous iron oxidation

***Corresponding author:**
Dongsheng Zhou
(2023009@zync.edu.cn)

Citation: Long J, Zhou D. Removal of antimonite by low-temperature Fe-modified biochar. *Asian J Water Environ Pollut.* 2026;23(3):026050027. doi: 10.36922/AJWEP026050027

Received: January 30, 2026

Revised: February 21, 2026

Accepted: February 24, 2026

Published online: April 22, 2026

1. Introduction

Antimony (Sb) is a toxic metalloid. It exerts toxic effects on living organisms by binding to sulfhydryl groups in proteins and enzymes, disrupting metabolic processes, and thereby interfering with enzyme activity.[1,2] The global average concentration of Sb in water is low (less than 1 $\mu g \cdot L^{-1}$); however, elevated concentrations of Sb have become ubiquitous in the environment due to widespread application of Sb and its compounds in various industrial processes.[3,4] Anthropogenic activities such as mining and smelting operations, coal and petroleum combustion, ammunition production, battery production, and polyethylene terephthalate esterification are considered the primary

sources of Sb pollution.[5,6] The concentrations of Sb in water and sediment around the Sb mining and smelting area (a typical Sb-contaminated area) are up to 29.4 mg·L^{-1} and 1163 mg·kg^{-1}, respectively, whereas in distant regions, the corresponding concentrations are often less than 5.0 mg·L^{-1} and 3.0 mg·kg^{-1}, respectively.[7] Sb exists primarily as antimonite (Sb(III)) and pentavalent antimony (Sb(V)) in the natural environment in the form of antimonous acid and antimonic acid, respectively. Sb(III) is approximately 10 times more toxic than Sb(V).[8] Furthermore, Sb(III) exhibits greater phytoavailability to crops,[9] making it more easily accumulated in the food chain and posing substantial risks to human health. Low-cost and environmentally friendly approaches for Sb(III) removal are urgently required.

As a low-cost and versatile adsorbent, biochar (BC) has been extensively studied for mitigating the toxicity of heavy metals (e.g., Sb) and associated ecological risks.[10,11] Recent studies have focused on Sb(III) removal from wastewater using BCs modified with iron (Fe), manganese compounds, and/or nano zero-valent Fe.[10-13] These BCs achieved effective Sb removal mainly through the dual effects of Sb(III) adsorption and oxidation. Numerous studies have consistently proposed that adsorption is a synergistic outcome of multiple mechanisms, with surface complexation emerging as a dominant pathway.[14,15] Specifically, the oxygen-containing functional groups, such as carbonyl (C=O), hydroxyl (–OH), and carboxyl (–COOH), present on BC surfaces form stable inner-sphere complexes with Sb(III) ions via ligand exchange or chelation reactions.[16] Fe-modified BCs, which incorporate crystalline Fe oxides (e.g., magnetite [Fe_3O_4], hematite, or amorphous Fe hydroxides) onto their surface or porous structure, further reinforce Sb(III) adsorption through the formation of surface complexes between Sb(III) and Fe oxide functional groups (e.g., Fe–O–H).[11,13] Furthermore, electrostatic attraction under acidic conditions and physical pore filling also contribute to Sb(III) adsorption. On the other hand, the oxidation of Sb(III) is mediated by reactive oxygen species (ROS) generated via the Fe redox cycle and electron transfer from the electron–donating capacity of BCs, driven by semiquinone radicals, and directly induced by oxygen-containing functional groups (e.g., –COOH, –OH, C=O) on the BC surface.[11,17-20]

Although the modified BCs mentioned above achieved efficient Sb(III) removal, research is heavily biased toward high-temperature BC (500–800 °C). These BCs exhibit high surface area, abundant microporosity, and crystalline Fe oxides, all of which contribute to efficient Sb(III) removal. However, high pyrolysis temperatures not only increase energy consumption but also reduce the abundance of surface functional groups, which are critical for the complexation and oxidation of Sb(III).[21] Moreover, the content of polycyclic aromatic hydrocarbons (PAHs) in BCs increases with increasing pyrolysis temperature, with a temperature range of 400–550 °C producing higher PAH contents.[22,23] Consequently, the application of high-temperature BCs for environmental remediation leads to both high energy consumption and an elevated risk of secondary environmental contamination. Therefore, to mitigate these drawbacks while harnessing the benefits of biochar, exploring low-temperature variants for Sb(III) removal is warranted.

In contrast, low-temperature BC produced at a pyrolysis temperature of ~300 °C has potential in agriculture due to its high hydrophilicity, loose macro-mesopore structure, nutrient-rich ash, and good ecological compatibility.[24-26] Moreover, low-temperature BC contains abundant oxygen-containing functional groups[27] and can be efficiently used to remove organic contaminants and heavy metals from the environment.[21,28,29] Compared with high-temperature BC, the research and application of low-temperature BC in environmental remediation, particularly for Sb(III) removal, remain underexplored. To address the gap, this study investigated the Sb(III) removal performance of low-temperature BC (300 °C) modified with Fe.

Soluble Sb(III) concentrations in Sb-contaminated water bodies, sediments, and soils were much lower than those in industrial wastewater, with the highest level being several mg·L^{-1}.[1] We hypothesize that the high content of oxygen-containing functional groups and Fe species in low-temperature BC might synergistically contribute to the effective removal of Sb(III), with the dominant mechanism shifting from functional group-mediated processes at low pH to Fe redox-mediated processes at high pH, thus making it a more energy-efficient candidate material for Sb(III) remediation in environmental media. The present study employed two types of Fe-modified BCs: ferric chloride ($FeCl_3$)-biomass co-pyrolyzed BC (FB), and $FeCl_3$-impregnated pristine BC (FBC), with the pristine BC (PBC) serving as the control. Rice straw was selected as the biomass feedstock for BC preparation because it is an abundant agricultural waste (ensuring low cost and sustainability) and has been proven to have great potential for remediating heavy metal-contaminated environments.

2. Materials and methods

2.1. Materials

Sb(III) stock solution was prepared by dissolving potassium antimony tartrate (Aladdin Biochemical Technology Co., Ltd., Shanghai, China) in ultrapure water. $FeCl_3$ (Macklin Bio-Chem Technology Co., Ltd., Shanghai,

China) was employed as the Fe source for the preparation of Fe-modified BC. All solutions used in the present study were prepared with ultrapure water (resistivity: 18.2 MΩ·cm^{-1}). Rice straw was collected from an Sb-free rural area in Hunan province, China. The collected rice straw was thoroughly rinsed with tap water, oven-dried at 80 °C, and subsequently cut into small segments for the preparation of pristine and Fe-modified BCs.

2.2. Biochar preparation and characterization

Rice straw pieces were heated from room temperature to 300 °C in a muffle furnace within 30 min and maintained at this temperature for 1 h to prepare the PBC. Two modification methods were employed for the preparation of Fe-modified BCs. In the first method, the BC was prepared according to He *et al.*[30] A 0.1 M $FeCl_3$ solution was prepared by dissolving an appropriate amount of $FeCl_3$ in ultrapure water. Rice straw biomass (10 g) was then added to the $FeCl_3$ solution (200 mL) at an Fe-to-biomass mass ratio of 0.1. The mixture was shaken for 24 h and subsequently sonicated for 2 h at 25 °C using a 40 kHz ultrasonic probe (Lichen, China) to enhance Fe loading. Afterward, the impregnated biomass was filtered, dried at 80 °C for ~24 h, and then co-pyrolyzed at 300 °C for 1 h to obtain Fe-modified BC, denoted as FB. In the other method, according to a previous study,[31] PBC (10 g) was added to a 0.1 M $FeCl_3$ solution (200 mL) to achieve an Fe-to-biochar mass ratio of 0.1, and the mixture was continuously shaken for 24 h. The BC was filtered out and dried at 80 °C for 24 h. The Fe-modified BC prepared using this approach was named FBC. All the BC samples were ground, passed through a 200-mesh sieve, and then sealed for use in subsequent experiments.

The pH values of the PBC, FB, and FBC were measured using a pH meter (PHS-3C, Leici Technology Co., Ltd., China) after mixing BC with deionized water at a standard ratio of 1:25 (m/v). Zeta (ζ) potentials were determined using a Zetasizer (Malvern Zetasizer Nano ZS90, United Kingdom), and the point of zero charge (pHPZC) was derived from the ζ potential–pH curve when ζ = 0. The Fe concentrations of BCs were measured using an atomic absorption spectrometer (AA-7800, Shimadzu, Japan) following closed high-pressure digestion with a 2:1 volume/volume (v/v) nitric acid and hydrofluoric acid (HNO_3–HF) mixture in a digestion system (MDS-6G, Lichen, China). The digestion program was set as follows: heating to 120 °C at 5 °C/min, holding for 30 min, then ramping to 180 °C at 3 °C/min and maintaining for 60 min. The morphologies of all three BCs were observed using a scanning electron microscope (SEM; ZEISS Sigma 300, Carl Zeiss AG, Germany) equipped with an energy-dispersive X-ray spectrometer (QUANTAX400, Bruker, Germany). The binding energies of carbon (C), oxygen (O), and Fe were detected by X-ray photoelectron spectroscopy (XPS; K-Alpha, Thermo Fisher Scientific, United States of America [USA]). The crystallinity of the BCs was determined by X-ray diffraction (XRD; Rigaku Ultima IV, Rigaku Corporation, Japan). After mixing the sample with potassium bromide, the surface functional groups of the BCs were measured using Fourier transform infrared spectroscopy (FTIR; Nicolet iS20, Thermo Fisher Scientific, USA) in the wavenumber range of 400–4000 cm^{-1}.

2.3. Antimonite removal by biochars: Adsorption kinetics and isotherms

The removal of Sb (III) relies on changes in aqueous Sb (III) concentration. Given that adsorption dynamics and isotherms are also established based on variations in aqueous Sb(III) concentration, batch adsorption experiments (both adsorption dynamics and isotherms) were conducted in the present study as a reliable method for characterizing Sb(III) removal. According to our 7-day preliminary experiment, the concentration of Sb(III) in BC suspension tended to stabilize at approximately 24 h. Therefore, Sb(III) adsorption experiments were conducted for 48 h. In all adsorption experiments, the BC-to-solution ratio was 1:250, the temperature was maintained at 25 °C, and the initial pH of the BC suspension was unadjusted, with measured values of 7.78, 2.45, and 2.41 in PBC, FB, and FBC, respectively. The initial Sb(III) concentration in the adsorption kinetics was 5 mg·L^{-1}, and the isotherm study employed a range of Sb(III) concentrations, including 0, 0.5, 1, 2, 4, 8, 16, 32, 64, and 100 mg·L^{-1}. At specific sampling times, the BC suspension was collected and filtered through 0.22-μm polyether sulfone membranes. The filtrate was preserved in 0.5 M citric acid to prevent further oxidation of Sb(III), and Sb(III) quantification was performed using an atomic fluorescence spectrometer (AFS; AFS-8900, Haiguang, China) within 24 h. Adsorption kinetics data derived from the dynamics of the aqueous Sb(III) concentrations were fitted using the pseudo-first-order and pseudo-second-order models. Additionally, the Langmuir and the Freundlich models were employed to fit the adsorption isotherm data. The mathematical equations for all these models are provided in the Appendix A.

2.4. Antimonite removal mechanisms: Adsorption experiments under various pH values

To elucidate the mechanisms underlying the effects of functional groups and Fe species of the BCs on Sb(III) removal, batch adsorption experiments were conducted under different pH conditions. The key experimental conditions were as follows: a BC-to-solution ratio of

1:250, an initial Sb(III) concentration of 5 mg·L^{-1}, and pH of 3, 7, and 10 for each BC. The designation of the adsorption experiments is shown in Table 1. The pH of the BC suspensions was adjusted and maintained by adding 0.1 M HNO_3 and/or 0.1 M sodium hydroxide. After 48 h of reaction, the aqueous solution and solid phases of the adsorption systems were separated by centrifugation.

Table 1. Designations of BC adsorption systems at different pH levels

Group/BC type	pH	Designation
PBC	3, 7, 10	PBC–3, PBC–7, PBC–10
FB	3, 7, 10	FB–3, FB–7, FB–10
FBC	3, 7, 10	FBC–3, FBC–7, FBC–10

Abbreviations: BC: Biochar; FB: Ferric chloride ($FeCl_3$)-biomass co-pyrolyzed biochar BC; FBC: $FeCl_3$-impregnated pristine BC; PBC: pristine BC.

The Sb and Fe species in the aqueous solution were analyzed using AFS and ferrozine colorimetry, respectively. The Sb(III) concentration was determined directly in a citric acid-preserved aqueous solution. The total Sb concentration was measured after pre-reduction with 10% thiourea for 15 min, and Sb(V) concentration was calculated as the difference between the total Sb concentration and Sb(III) concentration. For Fe quantification, aqueous solutions were reacted with ferrozine (Fe(II)) or ascorbic acid-ferrozine (total Fe) in an acetic acid-sodium acetate buffer for 15 min. Fe(II) and total Fe concentrations were measured by an ultraviolet-visible spectrophotometer (HD-UV90, Horde, Shandong, China) at 562 nm, and Fe(III) concentration was calculated as the total Fe concentration minus the Fe(II) concentration. Additionally, the separated solid phases were dried in a vacuum freeze-drying oven for 24 h. The Sb 3d and Fe 2p spectra of the solid phases were analyzed by XPS, and the proportions of the Sb and Fe species were analyzed by peak fitting using the XPSPEAK4.1 (https://xpspeak.software.informer.com/4.1/). The oxygen-containing functional groups on the surfaces of the solid phases were characterized by FTIR.

2.5. Data statistical analysis

All experimental containers were soaked in 8% nitric acid for more than 8 h and thoroughly rinsed with deionized water to eliminate potential contamination. All batch experiments were performed in triplicate, and the concentration data are presented as the mean value ± standard deviation. The AFS was recalibrated with a standard solution after every 20 samples to ensure detection accuracy. The XPS and XRD data were analyzed using XPSPeak 4.1 and MDI Jade 6 (https://www.icdd.com/mdi-jade/), respectively. All graphs were plotted using Origin Pro 8. One-way analysis of variance (ANOVA) was performed using SPSS (version 22.0, SPSS Inc., USA) to evaluate significant differences among treatments (n = 3). Prior to ANOVA, data normality and homogeneity of variance were verified using the Shapiro–Wilk test and Levene's test, respectively. Duncan's multiple range test was then used for post-hoc multiple comparisons to determine significant differences in aqueous Sb and Fe concentrations under two scenarios: (i) adsorption systems within the same group at different pH values; (ii) systems from different groups at the same pH.

3. Results

3.1. Characterization of biochars

The pH values of the PBC, FB, and FBC were 7.63, 2.56, and 2.42, respectively (Table 2). The notably lower pH of the FB and FBC could be attributed to the hydrolysis of $FeCl_3$. This process generates a significant quantity of hydrogen ions (H^+), thereby acidifying the Fe-modified BC.[12] The pHPZC values for PBC, FB, and FBC were 4.6, 6.1, and 5.7, respectively, demonstrating that the Fe modification increased the pHPZC of BC. The Fe content in PBC was 3.81 g·kg^{-1}, and those in the FB and FBC were 49.3 and 43.4 g·kg^{-1}, respectively, indicating the successful Fe modification for FB and FBC.

Table 2. Basic physicochemical properties of the three types of BCs

Properties	PBC	FB	FBC
pH	7.63	2.56	2.43
ζ potentials (pH = 7)	−3.44 mV	−2.44 mV	−2.13 mV
pHPZC	4.6	6.1	5.7
Fe content	3.81 g·kg^{-1}	49.3 g·kg^{-1}	43.4 g·kg^{-1}
C/O ratio	2.48	2.01	1.19

Abbreviations: ζ: Zeta; BC: Biochar; C/O: Carbon/oxygen; FB: Ferric chloride ($FeCl_3$)-biomass co-pyrolyzed BC; FBC: $FeCl_3$-impregnated pristine BC; Fe: Iron; PBC: Pristine BC; pHPZC: pH at the point of zero charge.

The SEM images at 1.00 k× magnification showed that the microscopic morphologies of the FB and FBC are relatively similar to that of PBC (Figure 1). Specifically, all the samples were composed of a mixture of larger, irregularly shaped fragments and smaller aggregated particles. Whereas images at 40 k× magnification revealed a large number of uniform particles aggregated on the solid surfaces of the FB and FBC, which may be related to Fe oxyhydroxides or recombined residual cellulose/hemicellulose. In contrast, the PBC surface was relatively flat and smooth. As shown in Figure 2, the Fe content increased from 0.47% in the PBC to 4.85% and 4.34%

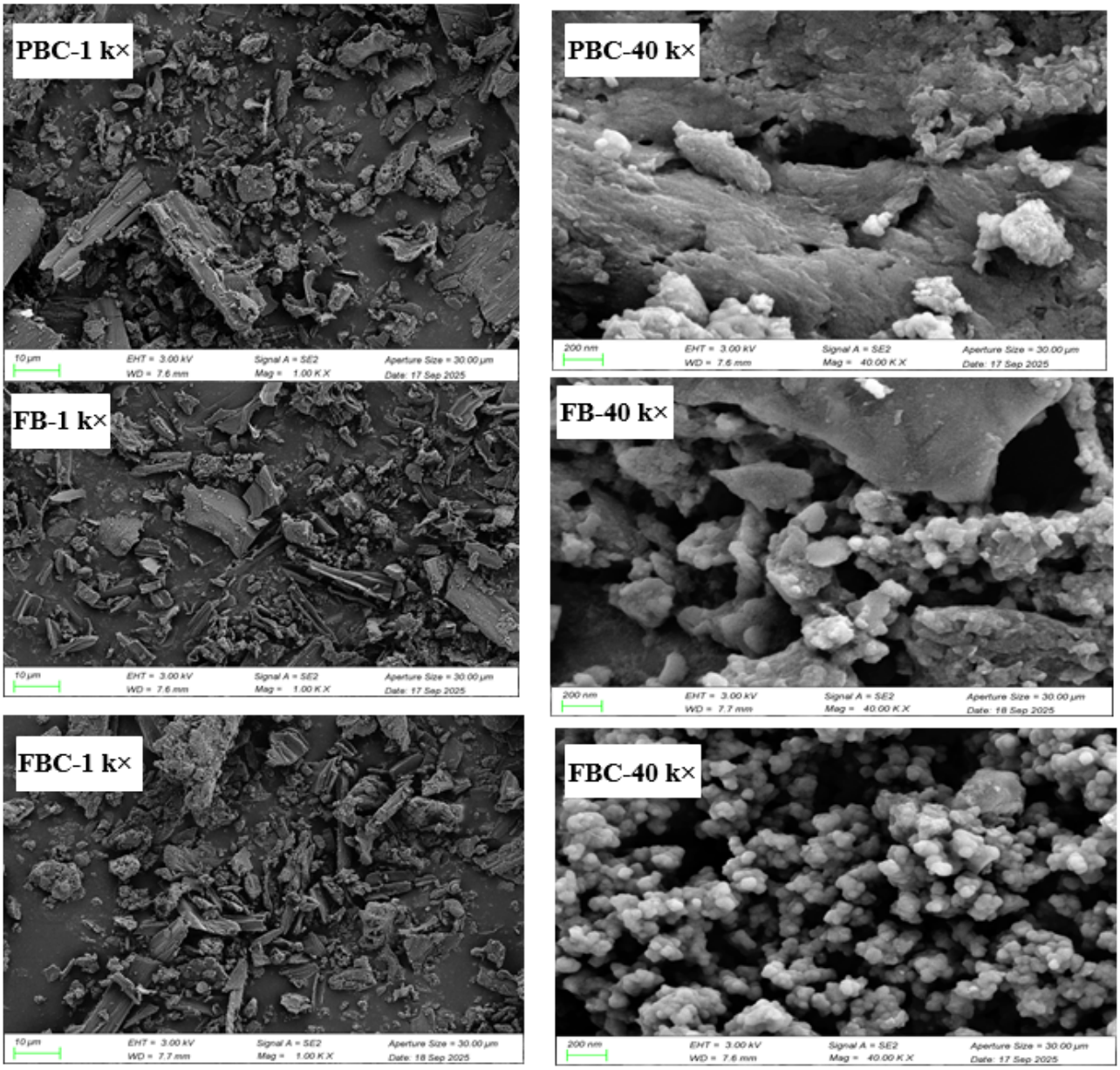

Figure 1. SEM images of three BCs at 1 k× (scale bar: 10 μm) and 40 k× (scale bar: 200 nm)
Abbreviations: BC: Biochar; EHT: Electron high tension; FB: Ferric chloride ($FeCl_3$)-biomass co-pyrolyzed BC; FBC: $FeCl_3$-impregnated pristine BC; Mag: Magnification; PBC: pristine BC; SEM: Scanning electron microscopy.

in the FB and FBC, respectively. Furthermore, the C/O ratios in the PBC, FB, and FBC were 2.48, 2.01, and 1.19, indicating that Fe modification increased the proportions of O in BCs.

The XRD patterns of the three BCs are shown in Figure 3. PBC and FBC exhibited similar diffraction peaks, with broad peaks at approximately 2θ = 16° and 23°. These peaks are likely to correspond to residual cellulose and/or hemicellulose in the rice straw BC.[32] In contrast, FB showed a broad diffraction hump, suggesting that Fe modification greatly altered the structure of this low-temperature BC. Characteristic diffraction peaks matching the standard PDF cards (PDF# 74–1877 and PDF# 70–0714) were observed in FB. Nevertheless, the XRD features suggest that the content of these Fe oxides was limited. In contrast, the Fe species introduced into the FBC were amorphous. The FTIR spectra of the three BCs are shown in Figure 4.

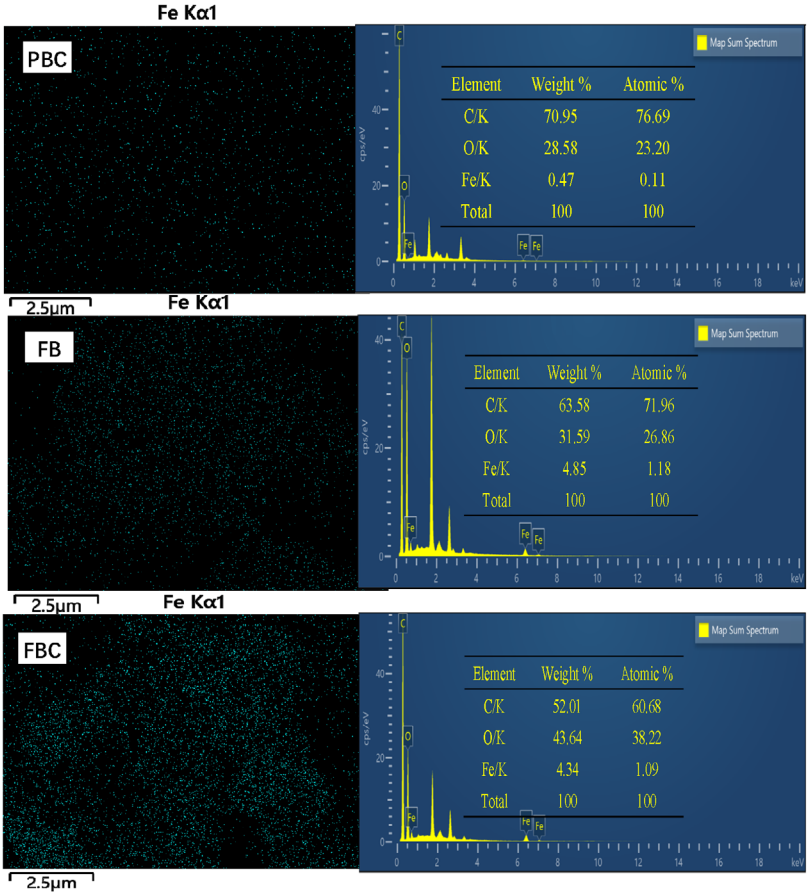

Figure 2. EDS images of three BCs. Scale bars: 2.5 μm; magnification: 40×.
Abbreviations: BC: Biochar; C: Carbon; EDS: Energy-dispersive X-ray spectroscopy; FB: Ferric chloride ($FeCl_3$)-biomass co-pyrolyzed BC; FBC: $FeCl_3$-impregnated pristine BC; Fe: Iron; K: Potassium; PBC: pristine BC.

All three BCs exhibited characteristic peaks, such as silicon (Si)–O–Si (450 cm^{-1}), aromatic hydrogen C–H (780 cm^{-1}), C–O (1136 cm^{-1}), C=C (1628 cm^{-1}), C=O (1736 cm^{-1}), and O–H (3401 cm^{-1}).[10,11,33] Furthermore, the peak intensities of C–H, C–O, C=C, and O–H vibrations were relatively lower in the FB than in the PBC and FBC. Additionally, several peaks (marked in red dashed zones) present in PBC and FBC were absent in the FB. No obvious Fe–O peak was observed in the two Fe-modified BCs; this may be due to the extremely weak Fe–O vibrational signals of the poorly crystalline Fe oxides in these BCs. Figure 5 shows the XPS spectra of C 1s, O 1s, and Fe 2p of the BCs. The C 1s analysis showed 56.9, 29.9, and 17.5% C=C in the PBC, FB, and FBC, respectively, and the O 1s spectra showed that the proportion of C=O in these BCs was 17.7, 42.1, and 44.6%, respectively. Furthermore, both the Fe(II) and Fe(III) components of Fe 2p were present in the FB and FBC; the Fe(II) accounted for 58.2 and 60.6% of the Fe 2p in these two BCs, respectively. These high proportions of Fe(II) are presumably formed during the low-temperature modification process, where free radicals in BC transfer electrons to $FeCl_3$.[17]

3.2. Antimonite removal by biochars

Figure 6 shows the dynamics of aqueous Sb(III) concentrations and the corresponding removal efficiencies during adsorption by the PBC, FB, and FBC. In the PBC adsorption systems, the Sb(III) concentration decreased from 2.61 $mg{\cdot}L^{-1}$ in the first 1 h to 0.16 $mg{\cdot}L^{-1}$ at 24 h, after which it remained stable for the rest of the experiment duration. For the FB and FBC adsorption systems, the Sb(III) concentrations decreased from 3.14 to 0.06 $mg{\cdot}L^{-1}$ (at 24 h) and from 2.26 to 0.04 $mg{\cdot}L^{-1}$ (at 34 h), respectively, indicating a relatively slower Sb(III) adsorption rate in the FBC system compared to those in the PBC and FB systems. Additionally, the Sb(III) removal efficiencies of the PBC, FB, and FBC increased from 47.8, 37.2, and 54.8% in the first 1 h to 95.8, 98.8, and 99.2% with adsorption

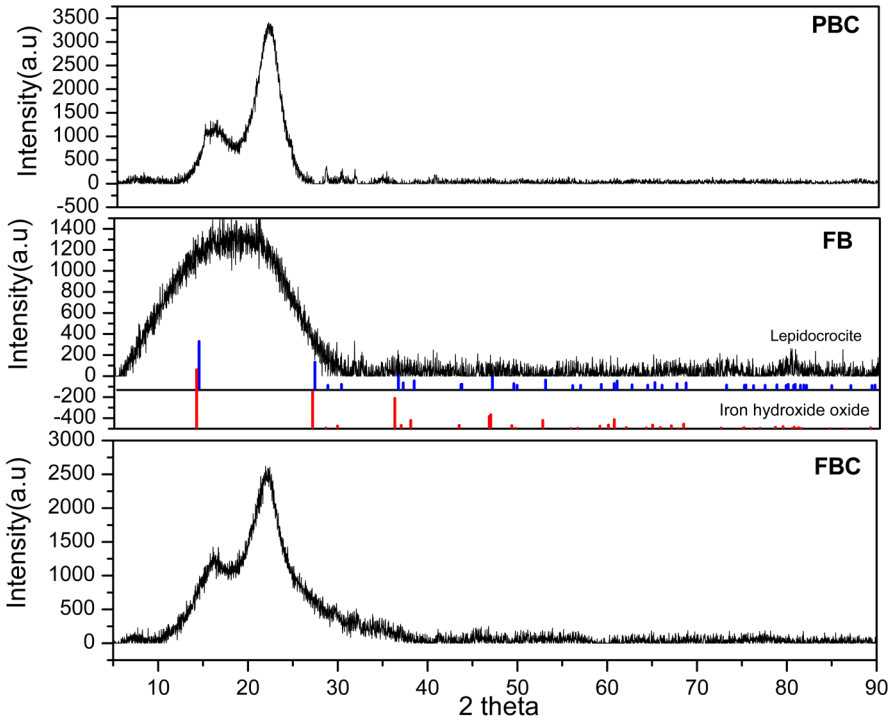

Figure 3. XRD patterns of the three BCs
Abbreviations: BC: Biochar; FB: Ferric chloride ($FeCl_3$)-biomass co-pyrolyzed BC; FBC: $FeCl_3$-impregnated pristine BC; PBC: pristine BC; XRD: X-ray diffraction.

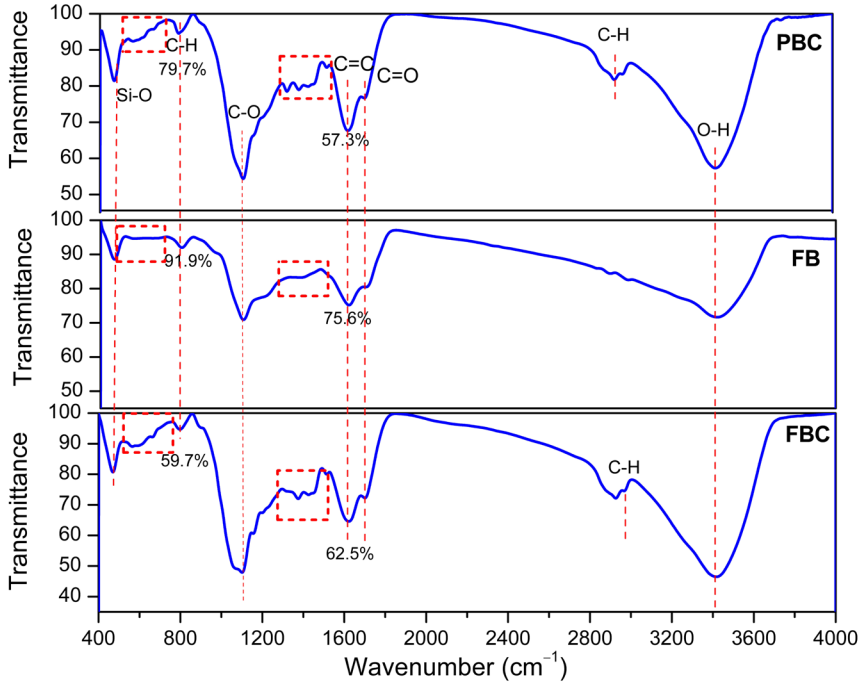

Figure 4. FTIR analysis of the three BCs
Abbreviations: BC: Biochar; C: Carbon; FB: Ferric chloride ($FeCl_3$)-biomass co-pyrolyzed BC; FBC: $FeCl_3$-impregnated pristine BC; FTIR: Fourier transform infrared spectroscopy; H: Hydrogen; O: Oxygen; PBC: pristine BC; Si: Silicon.

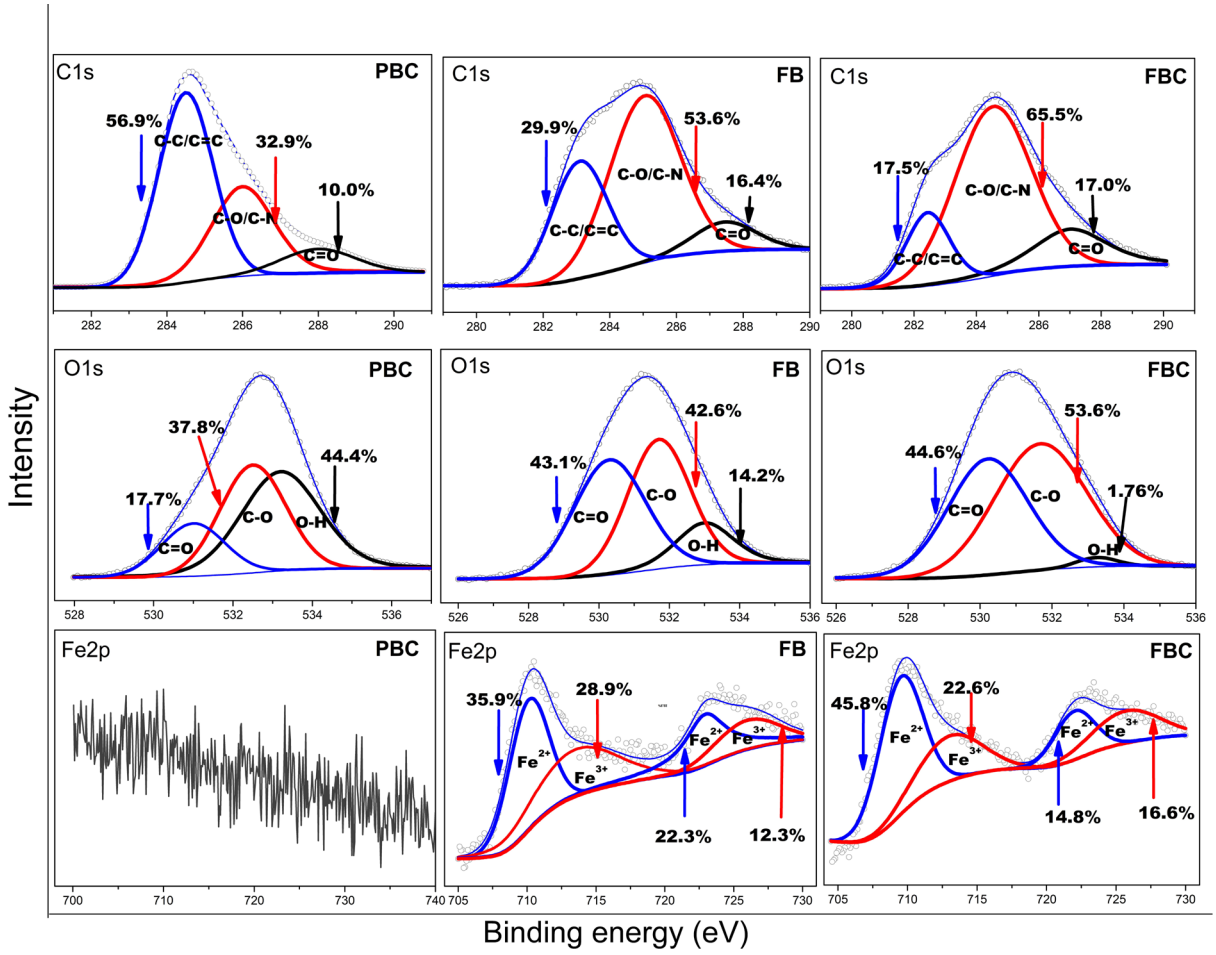

Figure 5. XPS of the three BCs
Abbreviations: BC: Biochar; C: Carbon; FB: Ferric chloride ($FeCl_3$)-biomass co-pyrolyzed BC; FBC: $FeCl_3$-impregnated pristine BC; Fe: Iron; O: Oxygen; PBC: pristine BC; XPS: X-ray photoelectron spectroscopy.

equilibrium achieved at 24, 24, and 34 h, respectively.

As shown in Figure 7A and Table 3, the equilibrium adsorption capacities (qe) of the PBC, FB, and FBC were 1.15, 1.20, and 1.20 mg·g^{-1}, respectively, indicating Fe modification slightly enhanced the Sb(III) adsorption capacity of the low-temperature BCs. The correlation coefficients (r^2) of the pseudo-first-order kinetic equation for PBC, FB, and FBC were 0.83, 0.52, and 0.47, respectively, while those of the pseudo-second-order kinetic equation were all 0.99. This confirmed that the pseudo-second-order model provided a better fit to the experimental data than the pseudo-first-order model, demonstrating that Sb(III) removal from the aqueous phase was dominated by chemical reactions rather than physical diffusion or mass transfer on the BC surface. According to Figure 7B and Table 4, the r^2 of the Langmuir model for the three BCs were 0.98, 0.98, and 0.95, and the corresponding maximum adsorption capacities (q_{max}) were 12.93, 9.01, and 14.58, respectively. Additionally, the chi-square (χ^2) values of the Langmuir model (54.90, 28.07, and 47.72 for the PBC, FB, and FBC) were significantly higher than those of the Freundlich model (2.84, 0.79, and 1.50 for the PBC, FB, and FBC). Thus, the Freundlich model fitted the Sb(III) adsorption data better for all three BCs, suggesting that Sb(III) adsorption occurred on heterogeneous surfaces with multiple types of adsorption sites, such as oxygen-containing functional groups, Fe oxides, and porous structures on the BCs.

3.3. Antimonite adsorption under different pH values

The aqueous Sb(III) concentrations in the adsorption experiments under different pH values for PBC, FB, and FBC were in the ranges of 0.16–0.47, 0.05–0.60, and 0.015–0.036 mg·L^{-1}, respectively (Figure 8). The residual total Sb

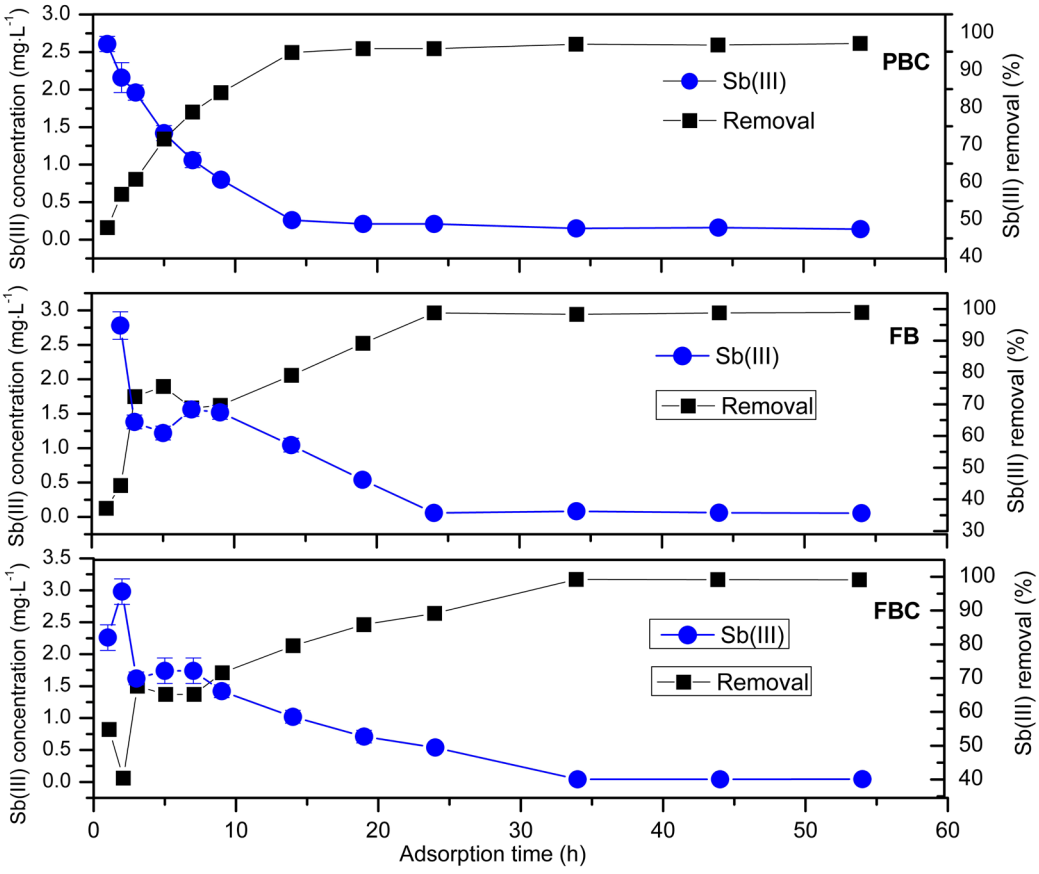

Figure 6. The dynamics of aqueous Sb(III) and its removal efficiency during kinetic adsorption
Abbreviations: BC: Biochar; FB: Ferric chloride ($FeCl_3$)-biomass co-pyrolyzed BC; FBC: $FeCl_3$-impregnated pristine BC; PBC: pristine BC; Sb(III): Antimonite.

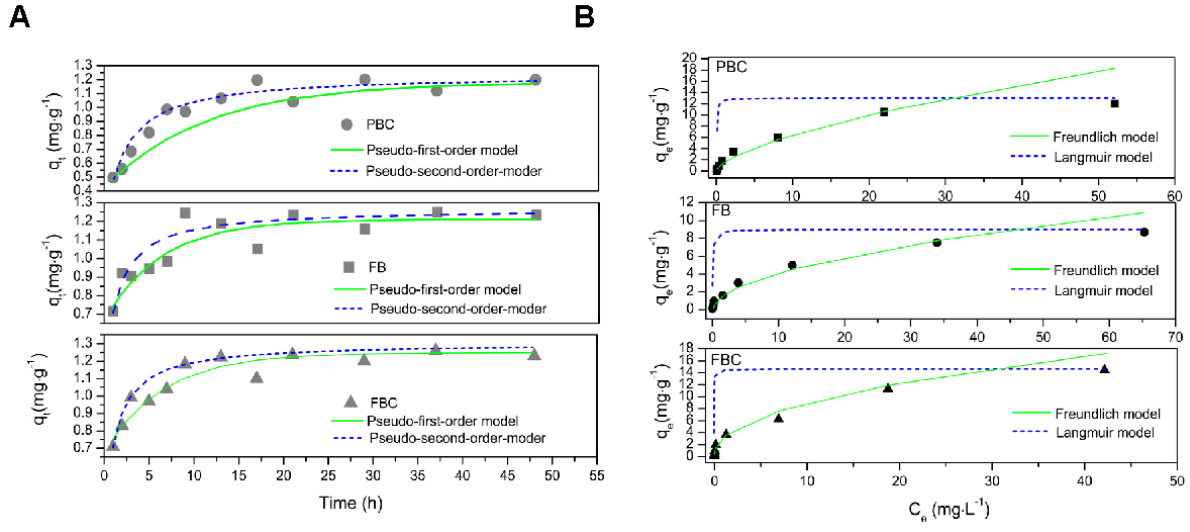

Figure 7. Sb(III) adsorption kinetics and isotherms by the three BCs (A: adsorption kinetics, B: adsorption isotherms)
Abbreviations: BC: Biochar; C_e: Equilibrium concentration of the adsorbate in solution; FB: Ferric chloride ($FeCl_3$)-biomass co-pyrolyzed BC; FBC: $FeCl_3$-impregnated pristine BC; PBC: pristine BC; q_e: Equilibrium adsorption capacities; q_t: Adsorption capacity at time t; Sb(III): Antimonite.

Table 3. Constants of adsorption kinetic models for the adsorption of Sb(III) by three types of BCs

BC type	Pseudo-first order model			Pseudo-second order model		
	K_1 (h^{-1})	q_e ($mg \cdot g^{-1}$)	r^2	K_2 ($g \cdot mg^{-1} h^{-1}$)	q_e ($mg \cdot g^{-1}$)	r^2
PBC	0.09	0.57	0.83	0.38	1.23	0.99
FB	0.17	0.56	0.52	0.64	1.26	0.99
FBC	0.16	0.47	0.47	0.74	1.27	0.99

Abbreviations: BC: Biochar; FB: Ferric chloride ($FeCl_3$)-biomass co-pyrolyzed BC; FBC: $FeCl_3$-impregnated pristine BC; K_1: Pseudo-first-order rate constant; K_2: Pseudo-second-order rate constant; PBC: ristine BC; q_e: Equilibrium adsorption capacities; r^2: Coefficient of determination; Sb(III): Antimonite.

Table 4. Constants of adsorption isotherms for the adsorption of Sb(III) by three types of BCs

	Langmuir isotherm				Freundlich isotherm			
BC type	q_{max} ($mg \cdot g^{-1}$)	b ($L \cdot mg^{-1}$)	r^2	χ^2	$k_f mg \cdot g^{-1} \cdot (L \cdot mg^{-1})^{1/n}$	1/n	r^2	χ^2
PBC	12.93	33.57	0.98	54.90	1.51	0.63	0.97	2.84
FB	9.01	17.33	0.98	28.07	1.26	0.52	0.97	0.79
FBC	14.58	92.52	0.95	47.73	3.08	0.46	0.95	1.50

Abbreviations: b: Langmuir adsorption equilibrium constant; BC: Biochar; FB: Ferric chloride ($FeCl_3$)-biomass co-pyrolyzed BC; FBC: $FeCl_3$-impregnated pristine BC; K_f: Freundlich adsorption capacity constant; PBC: pristine BC; q_{max}: Maximum adsorption capacities; r^2: Coefficient of determination; Sb(III): Antimonite. χ^2: Chi-square; 1/n: Freundlich adsorption intensity.

concentrations in the aqueous phase of these adsorption systems were 0.48–1.38, 0.65–0.85, and 0.17–1.03 $mg \cdot L^{-1}$, respectively. Based on the calculation of the measured Sb(III) and total Sb concentrations, the aqueous Sb(V) concentrations in the respective adsorption groups were in the ranges of 0.007–0.99, 0.045–0.79, and 0.13–1.01 $mg \cdot L^{-1}$. Within the PBC adsorption group, the lowest aqueous Sb(III) was observed at pH 7. By contrast, the minimum aqueous Sb(III) in the FB and FBC groups occurred at pH 10. Moreover, among the groups at pH 3, the aqueous Sb(III) in the PBC and FB were comparable (0.47 and 0.60 mg L^{-1}, respectively), whereas the aqueous Sb(III) in the FBC (0.036 mg L^{-1}) was significantly lower than in PBC and FB at the same pH ($p < 0.05$). At pH 10, the aqueous Sb(III) was in the order of PBC > FB > FBC. These results indicated that FBC exhibited optimal Sb(III) removal performance across the pH range 3–10. Aqueous Fe(II) was detected in all adsorption systems, with concentrations of 0.13–0.86, 0.87–6.37, and 0.71–6.76 $mg \cdot L^{-1}$ in the PBC, FB, and FBC groups, respectively (Figure 8). Clearly, the aqueous Fe(II) concentrations in the PBC group were much lower than those in the FB and FBC groups. Similarly, the total Fe concentrations in the PBC group (0.40–3.13 $mg \cdot L^{-1}$) were also considerably lower than those in the FB and FBC groups (2.53–14.9 and 2.01–15.4 $mg \cdot L^{-1}$, respectively).

The XPS analysis of Sb 3d in the solid phases (Figure 9) revealed that Sb in the solid phase existed exclusively as Sb(V) in all adsorption systems. Within each group, the area of the peak envelope of Sb 3d3/2 at lower pH was slightly larger than that at higher pH. For example, within the FBC adsorption group, the area of the peak envelope of Sb 3d3/2 at pH 3 was 9,136, whereas those at pH 7 and 10 were 8,702 and 8,062, respectively. FTIR analysis (Figure 10) of the solid phase revealed that, compared to the corresponding BC before adsorption, a red shift of functional groups such as C–O, C=C, C=O, and O–H was observed, and at pH 3, the intensities of these functional groups greatly decreased. After adsorption, Sb–O was observed in PBC–7, PBC–10, and all the FBCs. The XPS analysis of Fe 2p in the solid phase (Figure 11) showed both Fe(II) and Fe(III) were observed in the FB and FBC, and the proportion of Fe(II) decreased with increasing pH. More specifically, in the FB group, the proportion of Fe(II) decreased from 52.2% at pH 3 to 6.1% at pH 10. In the FBC group, as the pH increased from 3 to 10, the proportion of Fe(II) decreased from 56.4 to 18.5%.

4. Discussion

4.1. Antimonite removal by biochars

Given the low initial Sb(III) concentration (5 $mg \cdot L^{-1}$) and high BC-to-solution ratio (1:250) employed in the kinetic adsorption experiment, the Sb(III) removal efficiencies of PBC, FB, and FBC reached 95.8, 98.8, and 99.2%, respectively. The corresponding q_e values of these BCs in the kinetic adsorption experiment were relatively low, being only 1.15, 1.20, and 1.20 $mg \cdot g^{-1}$, respectively, which are lower than those of high-temperature BCs used for Sb(III) removal in previous studies.[10,15,18] However, the q_{max} of Sb(III) by these BCs in accordance with the Langmuir isotherm model calculation (r^2 were 0.98,

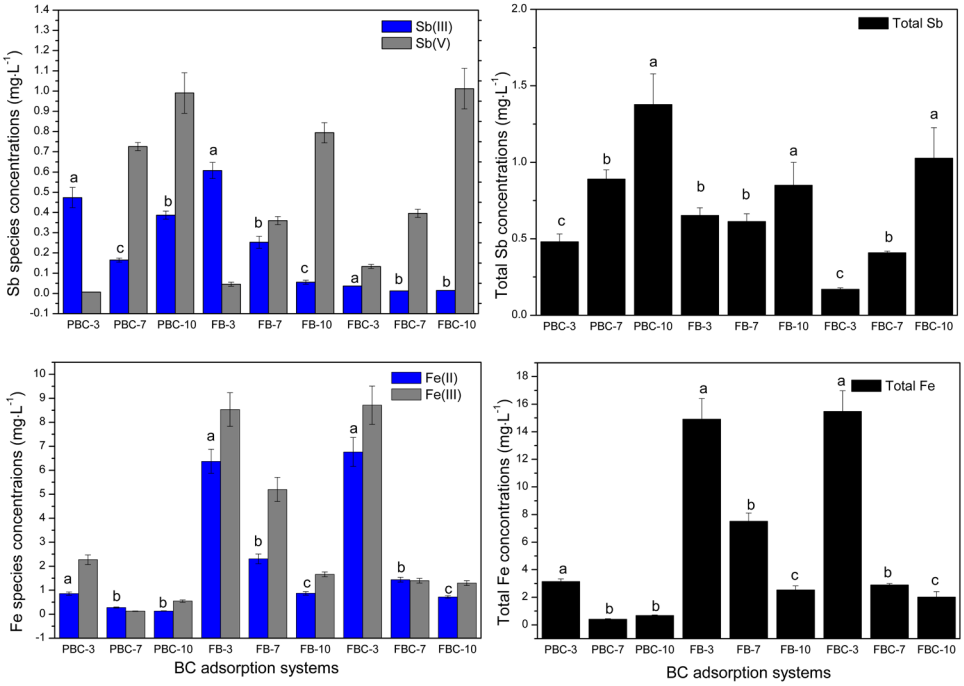

Figure 8. The species of Sb and Fe in the aqueous solution of the adsorption systems. Different lowercase letters (a, b, and c) indicate significant differences among treatments (one-way ANOVA followed by a post-hoc multiple comparison test, $p < 0.05$).
Abbreviations: BC: Biochar; FB: Ferric chloride ($FeCl_3$)-biomass co-pyrolyzed BC; FBC: $FeCl_3$-impregnated pristine BC; Fe: Iron; PBC: pristine BC; Sb: Antimony.

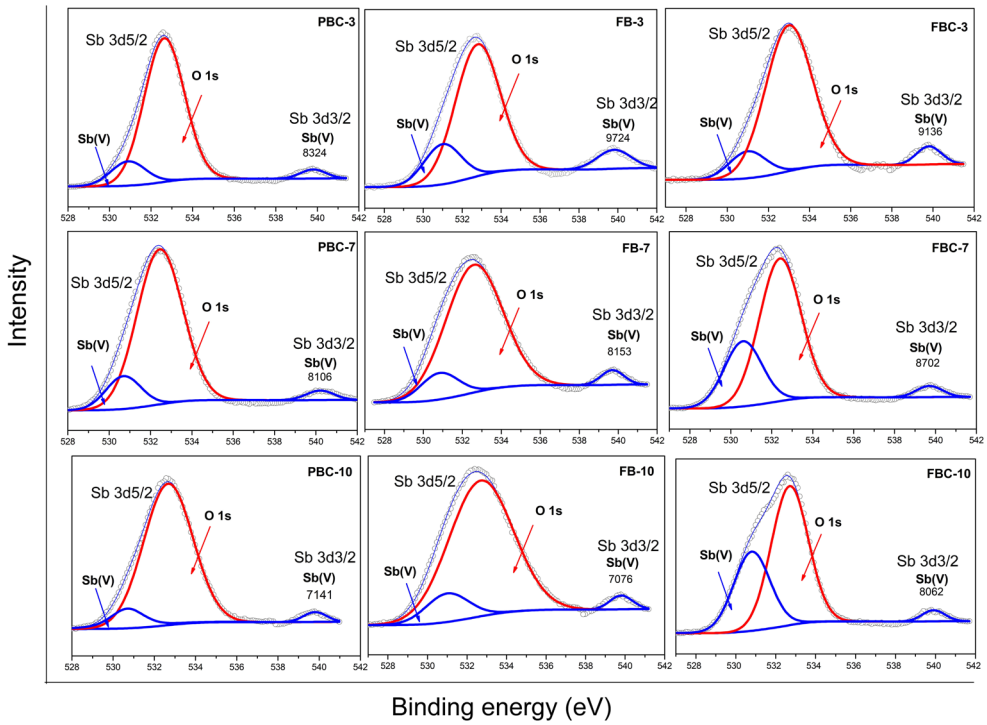

Figure 9. XPS analysis of Sb 3d for the solid phases from the adsorption systems
Abbreviations: BC: Biochar; FB: Ferric chloride ($FeCl_3$)-biomass co-pyrolyzed BC; FBC: $FeCl_3$-impregnated pristine BC; PBC: pristine BC; Sb: Antimony; XPS: X-ray photoelectron spectroscopy.

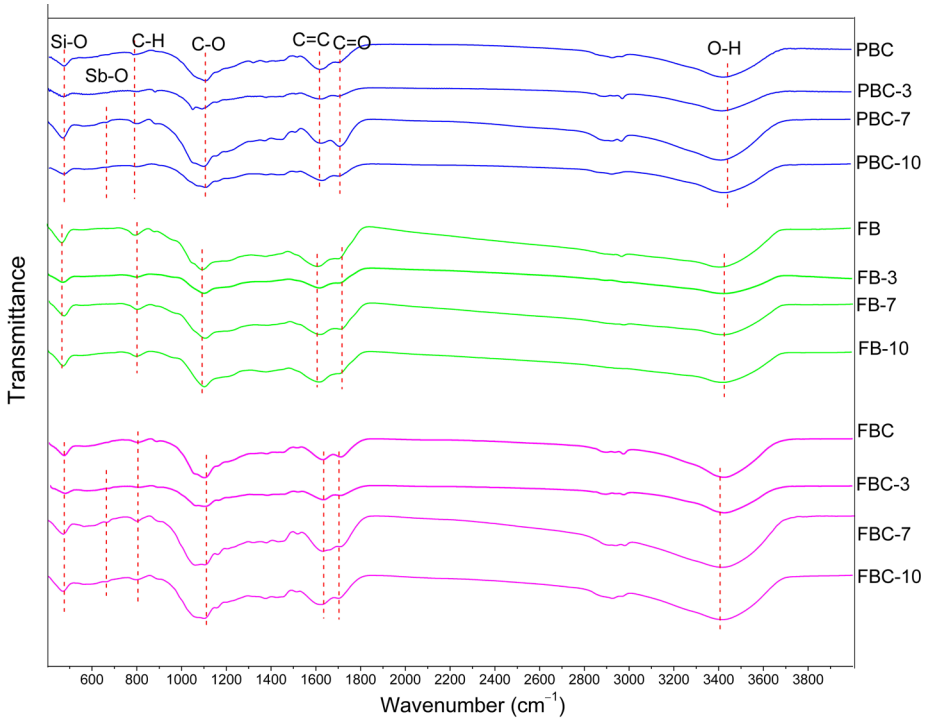

Figure 10. FTIR of solid phases from the adsorption systems
Abbreviations: BC: Biochar; C: Carbon; FB: Ferric chloride ($FeCl_3$)-biomass co-pyrolyzed BC; FBC: $FeCl_3$-impregnated pristine BC; FTIR: Fourier transform infrared spectroscopy; H: Hydrogen; O: Oxygen; PBC: pristine BC; Sb: Antimony; Si: Silicon.

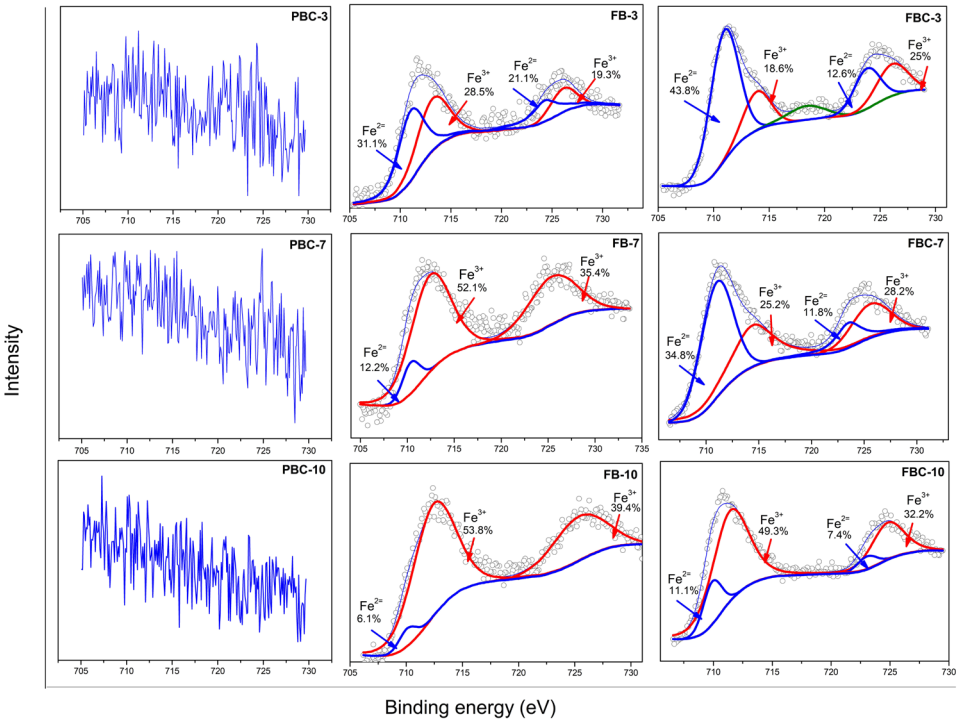

Figure 11. XPS analysis of Fe 2p for the solid phases from the adsorption systems
Abbreviations: BC: Biochar; FB: Ferric chloride ($FeCl_3$)-biomass co-pyrolyzed BC; FBC: $FeCl_3$-impregnated pristine BC; Fe: Iron; PBC: pristine BC; XPS: X-ray photoelectron spectroscopy.

0.98, and 0.95, respectively) were 12.9, 9.01, and 14.6 $mg \cdot g^{-1}$, respectively, which were much higher than the q_e in the kinetic adsorption experiment. This indicates that the BC dosage in adsorption systems can be reduced in future applications, thereby improving cost efficiency. Furthermore, because the Sb(III) adsorption by all BCs was well fitted by the pseudo-second-order and the Freundlich model, the adsorption process was assumed to be dominated by chemisorption (e.g., electron transfer and chemical bond formation)[17] on a heterogeneous surface-based multilayer,[34,35] which could be attributed to the uneven distribution of oxygen-containing functional groups and Fe-related sites on the BC surface.

4.2. Mechanisms of antimonite removal by biochars

In the adsorption systems of the PBC, FB, and FBC groups (at pH 3, 7, and 10), XPS analysis of Sb 3d for the solid phases from all adsorption systems revealed that Sb existed exclusively as Sb(V), and the aqueous Sb(V) concentrations were in the ranges of 0.007–0.99, 0.045–0.79, and 0.13–1.01 $mg \cdot L^{-1}$, respectively. These results demonstrated that Sb(III) adsorption and oxidation occurred concurrently in all three BC adsorption systems over the entire tested pH range. Thus, the Sb(III) removal by these low-temperature BCs was attributed to both the adsorption and oxidation.

As illustrated in Figure 9, the oxygen-containing functional groups (e.g., C=O, C–O, and O–H) on the BCs can form stable Sb(III)-complexes,[10,16] and this process was hypothesized to play a critical role in Sb(III) adsorption. The FTIR peaks corresponding to the C–H bending in aromatic compounds (at 780 cm^{-1}), the C=C stretching of conjugated alkene or aromatic compounds (1628 cm^{-1}), the C=O stretching in carbonyl-containing compounds (1736 cm^{-1}) collectively indicated that all the BCs exhibited significant equilibrium adsorption percentage (EAP), a key property underlying their redox activity.[11,33] This is because the conjugated π-system of aromatic rings provides a delocalized space for electron transfer, and the electron-deficient C in C=O groups enhances the ability to accept electrons from electron donors.[36,37] Therefore, Sb(III) can be efficiently oxidized through this EAP-mediated electron-transfer pathway. Additionally, compared to the corresponding BCs before adsorption, the red shift of these functional groups in the solid phases (such as C–O, C=O, and O–H) directly confirmed that these groups were involved in Sb(III) adsorption and/or oxidation. Notably, within each BC adsorption group, the intensities of the C–H, C–O, C=C, and O–H peaks of the solid phases at pH 3 were greatly decreased in comparison with the corresponding BCs before adsorption. Under acidic conditions, the conjugated π-systems of aromatic rings tend to exhibit an electron-deficient characteristic due to protonation effects, which enhances their tendency to accept electrons.[38] This suggests that Sb(III) removal under acidic conditions is largely attributable to these functional groups.

The detection of aqueous Fe(II) in the FB and FBC adsorption systems demonstrated that Fe was released from the solid phase.[39] This observation also implied that Fe(II) was formed during BC preparation or the Sb(III) removal process. The XPS analysis of Fe 2p in the BCs (Figure 5) provided direct evidence of Fe(II) formation during the BC preparation, which has been frequently observed in Fe-modified BCs in previous studies.[10,11,40] Compared with the Fe(II) proportion in the BCs before adsorption, those in the solid phases after adsorption decreased, which indicated that the Fe(II) oxidation co-occurred during Sb(III) adsorption/oxidation by the BCs. Studies have shown that the abiotic oxidation of Fe(II) by O_2 and other oxidants (e.g., hydrogen peroxide) can generate significant amounts of ROS.[41-43] A previous study explicitly showed that Sb oxidation occurs via Fe(II) oxygenation, with •OH serving as the primary ROS at acidic pH and Fe(IV) species being critical for Sb(III) oxidation at near-neutral pH.[44] Furthermore, radicals such as the 9,10-phenanthrene quinone radical in BC can transfer electrons to Fe(III), and then acquire electrons from Sb(III), thereby oxidizing Sb(III) to the less toxic Sb(V) even under anoxic conditions.[17] Thus, changes in the proportion of Fe(II) after adsorption in the present study indicated indirect oxidation of Sb(III) by the Fe(II) redox. Nevertheless, previous studies have reported the increases in Fe(II) content due to Sb(III) adsorption by BCs under acidic conditions.[10,11,15] This observation indicated that Sb(III) was adsorbed onto the Fe oxides of BCs, followed by electron transfer from Sb(III) to Fe(III), resulting in an increase in the proportion of Fe(II) after adsorption.[45,46] In the current study, XRD analysis of the BCs revealed limited formation of Fe oxides, and Sb(III) adsorption onto the Fe oxides of the solid phases is likely restricted. Thus, direct electron transfer between Fe(III) and Sb(III) was scarce. Furthermore, within each BC group, Fe(II) proportions in the solid phases at pH 3 were the highest, indicating that the Fe(II) oxidation was limited under the acidic conditions. Morgan and Lahav concluded that Fe(II) is the dominant Fe species in aerobic environments at pH below ~4,[47] which underpinned the findings of our study. On the contrary, within each BC adsorption group at pH 10, the Fe(II) proportions in the solid phases were extremely low. This phenomenon can be primarily ascribed to the rapid oxidation of Fe(II) by ambient oxygen under alkaline conditions.[47] Therefore, the indirect oxidation of Sb(III) by Fe(II) significantly contributed to Sb(III) removal at this pH. Whereas at pH 7, combined with the red shift of

functional groups and decreased proportion of Fe(II) in the solid phases, both functional groups and Fe(II) might be involved in Sb(III) adsorption/oxidation.

4.3. Biochar comparison and application prospects

Based on the q_{max} of Sb(III) by PBC, FB, and FBC (12.90, 9.01, and 14.57 mg·g^{-1}, respectively), it can be inferred that Fe modification enhanced Sb(III) removal capacity of FBC, while it decreased that of FB. According to previous studies, crystalline Fe oxides enhanced Sb(III) adsorption via electrostatic attraction and complexation reactions.[10] Although lepidocrocite and Fe oxyhydroxide were detected in FB, their low contents likely resulted in a negligible contribution to Sb(III) adsorption. Moreover, the pH values for the adsorption isotherm experiments were ~ 2.45, at which Sb(III) removal was primarily mediated by surface functional groups mentioned above. However, FTIR revealed a reduction in both the abundance and intensity of characteristic peaks in FB. Consequently, under acidic conditions (initial pH ~2.4), Sb(III) adsorption and oxidation processes associated with those functional groups were constrained, leading to low Sb(III) removal capacity. On the contrary, no crystalline Fe oxides were present in FBC; however, Fe modification elevated the levels of oxygen-containing functional groups, leading to a marked improvement in Sb(III) removal capacity under acidic conditions. Although FBC exhibited a higher q_{max} of Sb(III) (14.57 mg·g^{-1}) in comparison with FB, it was substantially lower than the reported capacities (64–106 mg·g^{-1}) of Fe-modified high-temperature BCs.[10-12] This discrepancy may be attributed to the limited contribution of key removal pathways in FBC, such as those involving Fe species (e.g., Fe_3O_4) for active sites, electrostatic attraction under acidic conditions, and physical pore-filling, which contributed to Sb(III) removal in Fe-modified high-temperature BCs.[11,13] Therefore, high-temperature BCs with higher adsorption capacity are suitable for industrial wastewater treatment.[48] Nevertheless, these two low-temperature BCs are preferentially suited for the remediation of waterbodies containing low levels of Sb(III).

It is worth noting that, within the FBC adsorption group with an initial Sb(III) concentration of 5 mg·L^{-1}, the residual aqueous Sb(III) concentrations ranged from 0.015 to 0.036 mg·L^{-1} as the pH increased from 3 to 10 (Figure 8). The extremely low residual Sb(III) concentrations confirmed that based on the relatively low Sb(III) concentration, FBC enabled efficient Sb(III) removal over a wide pH range (3–10), which can be attributed to the synergistic effects of its abundant functional groups and high Fe(II) content, with the former being primarily responsible at lower pH 3 and the latter exerting a dominant influence at higher pH 10. Unlike industrial wastewater with high Sb(III) concentrations and a controlled pH,[49,50] Sb-contaminated environmental matrices typically exhibit relatively low aqueous Sb(III) concentrations and variable pH. For instance, a previous study reported a total Sb concentration of 150 mg·kg^{-1} in the waterlogged soils around the world's largest Sb mine (Xikuangshan Sb mine), with the corresponding aqueous Sb(III) concentration measured at a mere 0.08 mg·L^{-1}.[51] Additionally, the average Sb(III) concentration in paddy field water near Sb mines is approximately 2.0 mg·L^{-1}.[1] Notably, Sb(III) exists predominantly under anaerobic conditions in the environmental matrices.[1] Under anaerobic acidic conditions, FBC was supposed to remove Sb(III) efficiently, since its surface functional groups, rather than oxygen, are mainly responsible for the adsorption process; however, under anaerobic alkaline conditions, the co-oxidation of Fe(II) and Sb(III) may be limited, and oxidation involving BC-derived radicals is likely to play a dominant role. Therefore, FBC demonstrates favorable adaptability and reliable Sb(III) removal performance across a wide pH range under typical anaerobic environmental conditions, highlighting its great potential for *in situ* remediation of Sb-contaminated paddy soils and natural water environments. Nevertheless, anions and humic substances in the environment affect the behavior of Sb(III) through competition, adsorption, complexation, and redox reactions.[52] It is necessary to clarify the impacts of these factors on Sb(III) removal by FBC prior to its application. In fact, due to its extremely low PAH content, high water-retention capacity, nutrient-supply capacity, and provision of microbial shelter, low-temperature biochar has been proven to be an excellent soil amendment.[28] Therefore, complemented by its versatile and efficient Sb(III) removal performance, FBC is a viable and promising *in situ* remediation material for Sb(III)-contaminated soils.

5. Conclusion

The maximum Sb(III) removal capacities of the low-temperature Fe-modified BCs were 9.01 and 14.57 mg·g^{-1}, respectively, lower than those of the high-temperature Fe-modified BC studied earlier. Sb(III) removal mechanisms by these two BCs were pH-dependent: at pH 3, the functional groups might be mainly responsible for the Sb(III) adsorption/oxidation, whereas the co-oxidation of Fe(II) and Sb(III) made a significant contribution to Sb(III) removal at pH 10. With an increased abundance of functional groups and higher Fe contents following $FeCl_3$ impregnation with pristine BC, FBC demonstrated versatile Sb(III) removal performance over a broad pH range of 3–10. As an energy-efficient and eco-friendly BC,

FBC exhibits significant potential for the remediation of low-concentration Sb(III)-contaminated water bodies, and as a promising *in situ* remediation material for Sb(III)-contaminated soils across the typical soil pH range. Future research should evaluate FBC's performance in real contaminated soil/water matrices, assess its long-term stability and reusability, and conduct pilot–scale remediation trials.

Acknowledgments

None.

Funding

This study was financially supported by Guizhou Provincial Basic Research Program (Natural Science) (No. Qiankehejichu-ZK[2024]yiban 691), and the Scientific Research Project of Zunyi Normal University (No. Zunshi BS[2023]17).

Conflict of interest

The authors declare that they have no competing interests.

Author contributions

Conceptualization: All authors
Formal analysis: Jiumei Long
Investigation: All authors
Methodology: Jiumei Long
Writing–original draft: Jiumei Long
Writing–review & editing: All authors

Availability of data

Data are available from the corresponding author upon reasonable request.

References

1. Zhang Y, O'Loughlin EJ, Kwon MJ. Antimony redox processes in the environment: A critical review of associated oxidants and reductants. *J Hazard Mater.* 2022;431:128607.

   doi: 10.1016/j.jhazmat.2022.128607

2. Li C, Ran Y, Wu P, *et al*. Antimony and arsenic migration in a heterogeneous subsurface at an abandoned antimony smelter under rainfall. *J Hazard Mater*. 2024;470:134156.

   doi: 10.1016/j.jhazmat.2024.134156

3. Herath I, Vithanage M, Bundschuh J. Antimony as a global dilemma: Geochemistry, mobility, fate and transport. *Environ Pollut*. 2017;223:545-559.

   doi: 10.1016/j.envpol.2017.01.057

4. Liu L, Supe Tulcan RX, He M, Ouyang W, Zhang Q, Huarez Yarleque, CM, *et al*. Antimony pollution threatens soils and riverine habitats across China: An analysis of antimony concentration changes and risks. *Crit Rev Environ Sci. Technol*. 2023;54(10):797-816.

   doi: 10.1080/10643389.2023.2279882

5. He M, Wang N, Long X, *et al*. Antimony speciation in the envFement: Recent advances in understanding the biogeochemical processes and ecological effects. *J Environ Sci*. 2019;75:14-39.

   doi: 10.1016/j.jes.2018.05.023

6. Bolan N, Kumar M, Singh E, *et al*. Antimony contamination and its risk management in complex environmental settings: A review. *EnvFe Int*. 2022;158:106908.

   doi: 10.1016/j.envint.2021.106908

7. Li L, Tu H, Zhang S, *et al*. Geochemical behaviors of antimony in mining-affected water environment (Southwest China). *Environ Geochem Health*. 2019;41(6):2397-2411.

   doi: 10.1007/s10653-019-00285-8

8. Filella M, Belzile N, Chen YW. Antimony in the environment: a review focused on natural waters: I. Occurrence. *Earth-Sci Rev*. 2002;57(1-2):125-176.

   doi: 10.1016/S0012-8252(01)00070-8

9. Long J, Tan D, Deng S, Li B, Ding D, Lei M. Antimony accumulation and Fe plaque formation at different growth stages of rice (Oryza sativa L.). *Environ Pollut*. 2019;249:414-422.

   doi: 10.1016/j.envpol.2019.03.042

10. Gao Y, Chen H, Fang Z, *et al*. Coupled sorptive and oxidative antimony (III) removal by Fe-modified biochar: Mechanisms of electron-donating capacity and reactive Fe species. *Environ Pollut*. 2023;337:122637.

    doi: 10.1016/j.envpol.2023.122637

11. Yao B, Li Y, Zeng W, *et al*. Synergistic adsorption and oxidation of trivalent antimony from groundwater using biochar-supported magnesium ferrite: Performances and mechanisms. *Environ Pollut*. 2023;323:121318.

    doi: 10.1016/j.envpol.2023.121318

12. Zhang L, Dong Y, Liu J, Liu C, Liu W, Lin H. The effect of co-pyrolysis temperature for Fe-biochar composites on their adsorption behavior of antimonite and antimonate in aqueous solution. *Bioresour Technol*. 2022;347:126362.

    doi: 10.1016/j.biortech.2021.126362

13. Zhang L, Yang D, Tao Y, *et al*. Efficiently simultaneous sorption and oxidation of antimonite on nitroso grafting-manganese loading binary-modified biochar from aqueous solution. *Sep Purif Technol*. 2024;337:126398.

    doi: 10.1016/j.seppur.2024.126398

14. Zhang L, Dong Y, Liu J, Liu W, Lu Y, Lin H. Promotion of higher synthesis temperature for higher-efficient removal of antimonite and antimonate in aqueous solution by Fe-loaded

porous biochar. *Bioresour Technol*. 2022;363:127889.

doi: 10.1016/j.biortech.2022.127889

15. Ji J, Xu S, Ma Z, Mou Y. Optimisation of preparation conditions and removal mechanism for trivalent antimony by biochar-supported nano zero-valent Fe. *EnvFe Technol Innov*. 2022;26:102240.

doi: 10.1016/j.eti.2021.102240

16. Dong Z, Zhou J, Huang T, *et al*. Effects of oxygen on the adsorption/oxidation of aqueous Sb (III) by Fe-loaded biochar: An X-ray absorption spectroscopy study. *Sci Total Environ*. 2022;846:157414.

doi: 10.1016/j.scitotenv.2022.157414

17. Wei D, Li B, Luo L, *et al*. Simultaneous adsorption and oxidation of antimonite onto nano zero-valent Fe sludge-based biochar: Indispensable role of reactive oxygen species and redox-active moieties. *J Hazard Mater*. 2020;391:122057.

doi: 10.1016/j.jhazmat.2020.122057

18. Chen H, Gao Y, Li J, Sun C, Sarkar B, Bhatnagar A. Insights into simultaneous adsorption and oxidation of antimonite [Sb (III)] by crawfish shell-derived biochar: spectroscopic investigation and theoretical calculations. *Biochar*. 2022;4(1):37.

doi: 10.1007/s42773-022-00161-2

19. Lai L, Liu X, Ren W, *et al*. Efficient removal of Sb (III) from water using β-FeOOH-modified biochar: synthesis, performance and mechanism. *Chemosphere*. 2023;311:137057.

doi: 10.1016/j.chemosphere.2022.137057

20. Chen H, Gao Y, El-Naggar A, *et al*. Enhanced sorption of trivalent antimony by chitosan-loaded biochar in aqueous solutions: characterization, performance and mechanisms. *J Hazard Mater.* 2022;425:127971.

doi: 10.1016/j.jhazmat.2021.127971

21. Chen Z, Zhang J, Huang, L Yuan Z, Li Z, Liu M. Removal of Cd and Pb with biochar made from dairy manure at low temperature. *J Integr Agric.* 2019;18(1):201-210.

doi: 10.1016/S2095-3119(18)61987-2

22. Buss W, Graham MC, MacKinnon G, Mašek O. Strategies for producing biochars with minimum PAH contamination. *J Anal Appl Pyrol.* 2016;119:24-30.

doi: 10.1016/j.jaap.2016.04.001

23. De la Rosa JM, Sánchez-Martín AM, Campos P, Miller AZ. Effect of pyrolysis conditions on the total contents of polycyclic aromatic hydrocarbons in biochars produced from organic residues: Assessment of their hazard potential. *Sci Total Environ*. 2019;667:578-585.

doi: 10.1016/j.scitotenv.2019.02.421

24. Ahmad M, Lee, SS, Lim JE, Lee SE, Cho JS, Moon DH. Speciation and phytoavailability of lead and antimony in a small arms range soil amended with mussel shell, cow bone and biochar: EXAFS spectroscopy and chemical extractions. *Chemosphere*. 2014;95:433-441.

doi: 10.1016/j.chemosphere.2013.09.077

25. Tomczyk A, Sokołowska Z, Boguta P. Biochar physicochemical properties: pyrolysis temperature and feedstock kind effects. *Rev Environ Sci Bio/Technol*. 2020;19(1):191-215.

doi: 10.1007/s11157-020-09523-3

26. Lin SL, Zhang H, Chen WH, Song M, Kwon EE. Low-temperature biochar production from torrefaction for wastewater treatment: A review. *Bioresour Technol.* 2023;387:129588.

doi: 10.1016/j.biortech.2023.129588

27. Gámiz B, Hall K, Spokas KA, Cox L. Understanding activation effects on low-temperature biochar for optimization of herbicide sorption. *Agronomy*. 2019;9(10):588.

doi: 10.3390/agronomy9100588

28. Gruss I, Twardowski JP, Latawiec A, Medyńska-Juraszek A, Królczyk J. Risk assessment of low-temperature biochar used as soil amendment on soil mesofauna. *Environ Sci Pollut Res.* 2019;26(18):18230-18239.

doi: 10.1007/s11356-019-05153-7

29. Guo F, Xu F, Cai R, *et al*. Enhancement of denitrification in biofilters by immobilized biochar under low-temperature stress. *Bioresour Technol.* 2022;347:126664.

doi: 10.1016/j.biortech.2021.126664

30. He R, Peng Z, Lyu H, Huang H, Nan Q, Tang J. Synthesis and characterization of an Fe-impregnated biochar for aqueous arsenic removal. *Sci Total Environ*. 2018;612:1177-1186.

doi: 10.1016/j.scitotenv.2017.09.016

31. Yang X, Shaheen SM, Wang J, *et al*. Elucidating the redox-driven dynamic interactions between arsenic and Fe-impregnated biochar in a paddy soil using geochemical and spectroscopic techniques. *J Hazard Mater.* 2022;422:126808.

doi: 10.1016/j.jhazmat.2021.126808

32. Yao W, Weng Y, Catchmark JM. Improved cellulose X-ray diffraction analysis using Fourier series modeling. *Cellulose*. 2020;27(10):5563-5579.

doi: 10.1007/s10570-020-03177-8

33. Zhang RY, Zheng XX, Chen BH, *et al*. Enhanced adsorption of sulfamethoxazole from aqueous solution by Fe-impregnated graphited biochar. *J Clean Prod.* 2020;256:120662.

doi: 10.1016/j.jclepro.2020.120662

34. Yanniotis, S, Blahovec, J. Model analysis of sorption isotherms. *LWT-Food Sci Technol*. 2009;42(10):1688-1695.

doi: 10.1016/j.lwt.2009.05.010

35. Tang J, Zhao B, Lyu H, Li D. Development of a novel pyrite/biochar composite (BM-FeS_2@BC) by ball milling for aqueous Cr(VI) removal and its mechanisms. *J Hazard Mater.* 2021;413:125415.

doi: 10.1016/j.jhazmat.2021.125415

36. Yan B, Niu C, Wang J. Analyses of levofloxacin adsorption on pretreated barley straw with respect to temperature: kinetics, π–π electron-donor–acceptor interaction and site energy distribution. *Environ Sci Technol.* 2017;51:8048-8056.

doi: 10.1021/acs.est.7b00327

37. Yang D, Li J, Luo L, Deng R, He Q, Chen Y. Exceptional levofloxacin removal using biochar-derived porous carbon sheets: Mechanisms and density-functional-theory calculation. *Chem Eng* J. 2020;387:124103.

doi: 10.1016/j.cej.2020.124103

38. Berryman OB, Johnson DW. Experimental evidence for interactions between anions and electron-deficient aromatic rings. *Chem Commun*. 2009;22:3143-3153.

doi: 10.1039/B823236A

39. Fan P, Sun Y, Qiao J, Imc L, Guan X. Influence of weak magnetic field and tartrate on the oxidation and sequestration of Sb(III) by zerovalent Fe: batch and semi-continuous flow study. *J Hazard Mater.* 2017;343:266-275.

doi: 10.1016/j.jhazmat.2017.09.041

40. Wang H, Guo W, Yin R, *et al*. Biochar-induced Fe (III) reduction for persulfate activation in sulfamethoxazole degradation: Insight into the electron transfer, radical oxidation and degradation pathways. *Chem Eng J.* 2019;362:561-569.

doi: 10.1016/j.cej.2019.01.053

41. Huang JZ, Jones A, Waite TD, *et al*. Fe(II) redox chemistry in the environment. *Chem. Rev*. 2021;121(13):8161-8233.

doi: 10.1021/acs.chemrev.0c01286

42. Zhang X, Fu Q, Hu H, Zhu J, Liu Y. Effects of Fe (II) on As (III) oxidation in Fe (II)-As (III) co-oxidation: Limiting and driving roles. *J Hazard Mater.* 2023;447:130790.

doi: 10.1016/j.jhazmat.2023.130790

43. Meng F, Tong H, Feng C, *et al*. Structural Fe (II)-induced generation of reactive oxygen species on magnetite surface for aqueous As (III) oxidation during oxygen activation. *Water Res*. 2024;252:121232.

doi: 10.1016/j.watres.2024.121232

44. Wang Y, Kong L, He M, *et al*. Mechanistic insights into Sb (III) and Fe (II) co-oxidation by oxygen and hydrogen peroxide: Dominant reactive oxygen species and roles of organic ligands. *Water Res*. 2023;242:120296.

doi: 10.1016/j.watres.2023.120296

45. Cheng Z, Lyu HH, Shen BX, Tian JY, Sun YF, Wu CF. Removal of antimonite (Sb(III)) from aqueous solution using a magnetic Fe-modified carbon nanotubes (CNTs) composite: experimental observations and governing mechanisms. *Chemosphere*. 2022;288:132581.

doi: 10.1016/j.chemosphere.2021.132581

46. Xu ZB, Wan ZH, Sun YQ, *et al*. Electroactive Fe-biochar for redox-related remediation of arsenic and chromium: distinct redox nature with varying Fe/carbon speciation. *J Hazard Mater.* 2022;430:128479.

doi: 10.1016/j.jhazmat.2022.128479

47. Morgan, B, Lahav, O. The effect of pH on the kinetics of spontaneous Fe (II) oxidation by O_2 in aqueous solution-basic principles and a simple heuristic description. *Chemosphere*. 2007;68(11):2080-2084.

doi: 10.1016/j.chemosphere.2007.02.015

48. Abhishek K, Parashar N, Patel M, *et al*. Recent advancements in antimony (Sb) removal from water and wastewater by carbon-based materials: a systematic review. *Environ Monit Assess*. 2023;195(6):758.

doi: 10.1007/s10661-023-11322-6

49. Xu S, Zhong Z, Liu W, Deng H, Lin Z. Removal of Sb(III) from wastewater by magnesium oxide and the related mechanisms. *Environ Res*. 2020;186:109489.

doi: 10.1016/j.envres.2020.109489

50. Chen W, Lin Z, Chen Z, Weng X, Owens G, Chen Z. Simultaneous removal of Sb(III) and Sb(V) from mining wastewater by reduced graphene oxide/bimetallic nanoparticles. *Sci Total Environ.* 2022;836:155704.

doi: 10.1016/j.scitotenv.2022.155704

51. Long J, Zhou D, Wang J, *et al*. Repeated inoculation of antimony resistant bacterium reduces antimony accumulation in rice plants. *Chemosphere*. 2023;327:138335.

doi: 10.1016/j.chemosphere.2023.138335

52. Ceriotti G, Amarasiriwardena D. A study of antimony complexed to soil-derived humic acids and inorganic antimony species along a Massachusetts highway. *Microchem J*. 2009;91(1):85-93.

doi: 10.1016/j.microc.2008.08.010

Appendix A

Appendix A.1.

The mathematical equations of the pseudo-first order rate model and the pseudo-second order rate model are expressed as follows:

$$q_t = q_e(1 - e^{-k_1 t}) \tag{A1}$$

$$q_t = \frac{k_2 q_e^2 t}{1 + k_2 q_e t} \tag{A2}$$

where q_t (mg·g^{-1}) and q_e (mg·g^{-1}) are the adsorbate adsorbed at any time and equilibrium time, respectively. K_1 (h^{-1}) and K_2 (g·mg^{-1} h^{-1}) are the first and second order rate constants, respectively.

Appendix A.2.

The mathematical equations of the Langmuir and the Freundlich are expressed as follows:

$$q_e = \frac{q_{max} b c_e}{1 + b c_e} \tag{A3}$$

$$q_e = k_f c_e^{1/n} \tag{A4}$$

where q_e (mg·g^{-1}) and q_{max} (mg·g^{-1}) are the adsorption capacity and the maximum adsorption capacity, respectively. b is the adsorption reaction constant (L·mg^{-1}), C_e is the equilibrium concentration of adsorbate (mg·L^{-1}), K_f and n are the empirical constants.